Particle-number projection in the finite-temperature mean-field approximation

P. Fanto,[1] Y. Alhassid,[1] and G. F. Bertsch[2]
[1]*Center for Theoretical Physics, Sloane Physics Laboratory, Yale University, New Haven, Connecticut 06520, USA*
[2]*Department of Physics and Institute for Nuclear Theory, Box 351560, University of Washington, Seattle, Washington 98915, USA*
(Received 9 January 2017; published 7 July 2017)

Finite-temperature mean-field theories, such as the Hartree–Fock (HF) and Hartree–Fock–Bogoliubov (HFB) theories, are formulated in the grand-canonical ensemble, and their applications to the calculation of statistical properties of nuclei such as level densities require a reduction to the canonical ensemble. In a previous publication [Y. Alhassid *et al.*, Phys. Rev. C **93**, 044320 (2016)], it was found that ensemble-reduction methods based on the saddle-point approximation are not reliable in cases in which rotational symmetry or particle-number conservation is broken. In particular, the calculated HFB canonical entropy can be unphysical as a result of the inherent violation of particle-number conservation. In this work, we derive a general formula for exact particle-number projection after variation in the HFB approximation, assuming that the HFB Hamiltonian preserves time-reversal symmetry. This formula reduces to simpler known expressions in the HF and Bardeen–Cooper–Schrieffer (BCS) limits of the HFB. We apply this formula to calculate the thermodynamic quantities needed for level densities in the heavy nuclei ^{162}Dy, ^{148}Sm, and ^{150}Sm. We find that the exact particle-number projection gives better physical results and is significantly more computationally efficient than the saddle-point methods. However, the fundamental limitations caused by broken symmetries in the mean-field approximation are still present.

DOI: 10.1103/PhysRevC.96.014305

I. INTRODUCTION

Finite-temperature mean-field approximations, in particular the finite-temperature Hartree–Fock (HF) and Hartree–Fock–Bogoliubov (HFB) approximations [1,2], are commonly used in the calculation of statistical properties of nuclei such as level densities [3]. These approximations are computationally efficient and therefore suitable for global studies of nuclear properties.

The appropriate ensemble to describe the nucleus is the canonical ensemble with fixed numbers of protons and neutrons. However, the finite-temperature HF and HFB approximations are formulated in the grand-canonical ensemble. It is therefore necessary to carry out a reduction to the canonical ensemble to restore the correct proton and neutron numbers. This reduction is usually carried out in the continuous saddle-point approximation, which treats the particle number as a continuous variable [4–6]. The accuracy of finite-temperature mean-field approximations was recently benchmarked [7] against shell-model Monte Carlo (SMMC) [8–10] results, which are accurate up to statistical errors, and significant problems were identified with this continuous saddle-point approach. In particular, the continuous saddle-point approximation breaks down when the particle-number fluctuations are small. These problems were addressed in Ref. [7] by the introduction of the discrete Gaussian (DG) approximations. Specifically, in Ref. [7] two DG approximations were introduced, which we label DG1 and DG2 and discuss in detail in Sec. III. In these approximations, the saddle-point correction to the grand-canonical partition function is given by a sum over discrete Gaussians (in particle number). This overcomes a divergence in the continuous saddle-point approximation at low temperatures in the HF approximation, but still gives an unphysical negative value of the canonical entropy in the low-temperature limit of the HFB.

Here, we study the restoration of particle-number conservation in the HFB by means of an exact particle-number projection [11,12]. In particular, we use a projection after variation (PAV) method, in which the projection operator is applied to the grand-canonical mean-field solution. We refer to this particle-number PAV method as the particle-number projection (PNP). In this procedure, we determine the approximate canonical partition function by taking a trace of the grand-canonical mean-field density operator over a complete basis of many-particle states with the correct particle number. In contrast, in the DG approximations, the grand-canonical partition function is multiplied by an approximate correction factor. A general formalism for PNP was presented in Ref. [12], and an alternate but equivalent formalism was derived in Ref. [13]. However, in the HFB case the application of the general formula is limited by a sign ambiguity. Moreover, there has been no systematic assessment of the accuracy of PNP in finite-temperature mean-field theories.

In this article, we derive a general expression for PNP in the HFB approximation, assuming only that the HFB Hamiltonian is invariant under time reversal. We then show how this expression reduces to known formulas for the special cases of the HF and the Bardeen–Cooper–Schrieffer (BCS) approximations. We apply this method to three even-even nuclei in the rare-earth region: (i) a strongly deformed nucleus with weak pairing (^{162}Dy), (ii) a spherical nucleus with strong pairing (^{148}Sm), and (iii) a transitional deformed nucleus with non-negligible pairing (^{150}Sm). The results from the PNP are compared with results from the DG approximations and the SMMC method.

The outline of this article is as follows: In Sec. II, we derive a general expression for the particle-number projected HFB partition function in the case where the HFB Hamiltonian is time-reversal invariant and show how this expression simplifies in the HF and BCS limits. In Sec. III, we discuss

the DG approximations and describe how we calculate the approximate canonical thermal energy, entropy, and state density from the particle-number projected partition function. In Sec. IV, we apply the PNP formula to three heavy nuclei and compare the results with those from the DG approximations and with SMMC results. Finally, in Sec. V, we summarize our findings and provide an outlook for future work. The computer codes for the canonical reductions and the data files to generate the results described here are provided in the Supplemental Material depository for this article [14].

II. PARTICLE-NUMBER PROJECTION IN HARTREE–FOCK–BOGOLIUBOV APPROXIMATION

We assume a nuclear Hamiltonian in Fock space spanned by a set of N_s single-particle orbitals k ($k = 1, \ldots, N_s$) with a one-body part described by the matrix t and an antisymmetrized two-body interaction $\bar{v}$,

$$\hat{H} = \sum_{ij} t_{ij} a_i^\dagger a_j + \frac{1}{4} \sum_{ijkl} \bar{v}_{ijkl} a_i^\dagger a_j^\dagger a_l a_k, \tag{1}$$

where $a_k^\dagger$ and a_k are, respectively, creation and annihilation operators of the single-particle states k. For nuclei with strong pairing condensates, the appropriate mean-field theory is the HFB approximation. The HFB Hamiltonian can be written in matrix notation as [11]

$$\hat{H}_{\rm HFB} - \mu \hat{N} = \frac{1}{2}(a^\dagger a) \begin{pmatrix} h-\mu & \Delta \\ -\Delta^* & -(h^*-\mu) \end{pmatrix} \begin{pmatrix} a \\ a^\dagger \end{pmatrix} + \frac{1}{2}{\rm tr}\,(h-\mu), \tag{2}$$

where μ is the chemical potential, $h = t + \bar{v}\varrho$ is the density-dependent single-particle Hamiltonian, and $\Delta_{ij} = \sum_{ijkl} \bar{v}_{ijkl}\kappa_{kl}/2$ is the pairing field, with ϱ being the one-body density and κ the pairing tensor. The $2N_s \times 2N_s$ matrix in Eq. (2) can be diagonalized by a unitary transformation to the quasiparticle basis $\alpha_k, \alpha_k^\dagger$.

We assume that the HFB Hamiltonian in Eq. (2) is invariant under time reversal, and thus its quasiparticle states come in time-reversed pairs $|k\rangle$ and $|\bar{k}\rangle$ with degenerate energies $E_k = E_{\bar{k}}$.[1] The Bogoliubov transformation that defines the quasiparticle basis can then be fully expressed by

$$\begin{pmatrix} \alpha_k \\ \alpha_{\bar{k}}^\dagger \end{pmatrix} = \mathcal{W}^\dagger \begin{pmatrix} a_k \\ a_{\bar{k}}^\dagger \end{pmatrix}, \quad \mathcal{W} = \begin{pmatrix} \mathcal{U} & -\mathcal{V} \\ \mathcal{V} & \mathcal{U} \end{pmatrix}, \tag{3}$$

where k runs over half the number of single-particle states from 1 to $N_s/2$. In the following, we denote these states by $k > 0$. $\mathcal{W}$ is an $N_s \times N_s$ unitary matrix, in contrast with the general Bogoliubov transformation matrix which is a $2N_s \times 2N_s$-dimensional matrix [11].

[1]If the condensate is also axially symmetric, the angular momentum m about the symmetry axis is conserved. If this is the case, we choose the k states to have positive signature, i.e., $m = 1/2, -3/2, 5/2, -7/2, \ldots$, and $\bar{k}$ states have negative signature $m = -1/2, 3/2, -5/2, 7/2, \ldots$.

Using $E_k = E_{\bar{k}}$, the HFB Hamiltonian in Eq. (2) can be rewritten as

$$\hat{H}_{\rm HFB} - \mu \hat{N} = \sum_{k>0} E_k (\alpha_k^\dagger \alpha_k - \alpha_{\bar{k}} \alpha_{\bar{k}}^\dagger) + \frac{1}{2}{\rm tr}\,(h-\mu). \tag{4}$$

In a more compact notation

$$\hat{H}_{\rm HFB} - \mu \hat{N} = \xi^\dagger \mathcal{E} \xi + \tfrac{1}{2}{\rm tr}\,(h-\mu), \tag{5}$$

where $\xi^\dagger = (\alpha_{k_1}^\dagger, \ldots, \alpha_{k_{N_s/2}}^\dagger, \alpha_{\bar{k}_1}, \ldots, \alpha_{\bar{k}_{N_s/2}})$ and

$$\mathcal{E} = \begin{pmatrix} E & 0 \\ 0 & -E \end{pmatrix}. \tag{6}$$

The matrix E is the diagonal matrix of the HFB quasiparticle energies E_k ($k = 1, \ldots, N_s/2$). Similarly, the number operator $\hat{N}$ can be written as

$$\hat{N} = \sum_{k>0} (a_k^\dagger a_k + a_{\bar{k}}^\dagger a_{\bar{k}}) = \sum_{k>0} (a_k^\dagger a_k - a_{\bar{k}} a_{\bar{k}}^\dagger) + \frac{N_s}{2} = \xi^\dagger (\mathcal{W}^\dagger \mathcal{N} \mathcal{W}) \xi + \frac{N_s}{2}, \tag{7}$$

where

$$\mathcal{N} = \begin{pmatrix} 1 & 0 \\ 0 & -1 \end{pmatrix}, \tag{8}$$

and where we have used the transformation in Eq. (3).

The particle-number-projected HFB partition function is defined by $Z_N^{\rm HFB} = {\rm Tr}[\hat{P}_N e^{-\beta(\hat{H}_{\rm HFB} - \langle \hat{V} \rangle)}]$, where $\hat{P}_N$ is the operator that projects any many-particle state in Fock space onto the Hilbert space of N-particle states, and $\hat{V}$ is the two-body interaction of the Hamiltonian (1). For a finite single-particle model space of dimension N_s, $\hat{P}_N$ can be expressed as a discrete Fourier sum over N_s quadrature angles $\varphi_n = 2\pi n/N_s$

$$Z_N^{\rm HFB} = \frac{e^{-\beta\mu N}}{N_s} \sum_{n=1}^{N_s} e^{-i\varphi_n N} \zeta_n^{\rm HFB}, \tag{9}$$

where

$$\zeta_n^{\rm HFB} = e^{\beta\langle \hat{V} \rangle} {\rm Tr}[e^{i\varphi_n \hat{N}} e^{-\beta(\hat{H}_{\rm HFB} - \mu \hat{N})}], \tag{10}$$

and μ is the chemical potential determined in the grand-canonical ensemble. The subtraction of $\langle \hat{V} \rangle = {\rm tr}\,(\varrho\bar{v}\varrho)/2 + {\rm tr}\,(\kappa^\dagger \bar{v} \kappa)/4$ accounts for the double counting of the interaction terms and ensures the thermodynamic consistency of the HFB in the grand-canonical ensemble. Because of the nonzero pairing gap Δ in Eq. (2), $\hat{H}_{\rm HFB}$ and $\hat{N}$ do not commute.

Using Eqs. (5) and (7), we can rewrite (10) as

$$\zeta_n^{\rm HFB} = e^{-\beta U_0} e^{i\varphi_n N_s/2} {\rm Tr}[e^{i\varphi_n \xi^\dagger (\mathcal{W}^\dagger \mathcal{N} \mathcal{W}) \xi} e^{-\beta \xi^\dagger \mathcal{E} \xi}], \tag{11}$$

where $U_0 = {\rm tr}\,(h-\mu)/2 - \langle \hat{V} \rangle$. To evaluate the trace in Eq. (11), we use the group property of the exponentials of one-body fermion operators written in quadratic form. This property states that the product of two such group elements is another group element

$$e^{\xi^\dagger \mathcal{A} \xi} e^{\xi^\dagger \mathcal{B} \xi} = e^{\xi^\dagger \mathcal{C} \xi}, \tag{12}$$

where the matrix $\mathcal{C}$ is determined from the single-particle representation of the group

$$e^{\mathcal{A}}e^{\mathcal{B}} = e^{\mathcal{C}}. \tag{13}$$

Applying this property to Eq. (11), we can rewrite it in the form

$$\zeta_n^{\rm HFB} = (-)^n e^{-\beta U_0}{\rm Tr}[e^{\xi^\dagger \mathcal{C}_n(\beta)\xi}], \tag{14}$$

where the matrix $\mathcal{C}_n(\beta)$ is determined from

$$e^{\mathcal{C}_n(\beta)} = e^{i\varphi_n \mathcal{W}^\dagger \mathcal{N}\mathcal{W}} e^{-\beta\mathcal{E}} = \mathcal{W}^\dagger e^{i\varphi_n \mathcal{N}}\mathcal{W}e^{-\beta\mathcal{E}}. \tag{15}$$

Using the formula for the trace of the exponential of a one-body fermionic operator (see Appendix A), we find

$$\zeta_n^{\rm HFB} = (-)^n e^{-\beta U_0}\det(1 + e^{\mathcal{C}_n(\beta)}). \tag{16}$$

Combining Eq. (16) with Eq. (15), we obtain the final expression

$$\zeta_n^{\rm HFB} = (-)^n e^{-\beta U_0}\det(1 + \mathcal{W}^\dagger e^{i\varphi_n \mathcal{N}}\mathcal{W}e^{-\beta\mathcal{E}}), \tag{17}$$

where the matrices $\mathcal{W}$, $\mathcal{E}$, and $\mathcal{N}$ are given, respectively, by Eqs. (3), (6), and (8).

Equation (17) is a general formula that applies when the HFB Hamiltonian is time-reversal invariant and thus the quasiparticle energies come in degenerate time-reversed pairs $E_k = E_{\bar{k}}$. A formula valid for the most general case can be derived in a similar fashion by using $\xi'^\dagger = (\alpha_k^\dagger\ \alpha_k\ \alpha_{\bar{k}}^\dagger\ \alpha_{\bar{k}})$ (where $k = 1, \ldots, N_s/2$) and making the dimension of the relevant matrices $2N_s \times 2N_s$ [12]. However, the final expression for $\zeta_n^{\rm HFB}$, given in Eq. (3.46) of Ref. [12], involves a square root of a determinant. This square root leads to a sign ambiguity that is difficult to resolve. The method discussed here eliminates this sign ambiguity completely for the case in which the HFB Hamiltonian is time-reversal invariant by working with matrices of reduced dimension $N_s \times N_s$.

Equation (17) becomes numerically unstable at large β. The reason for this instability can be seen in Eq. (15). At large β, the diverging scales in the diagonal matrix $e^{-\beta\mathcal{E}}$ will dominate the smaller scales in the matrix product $\mathcal{W}^\dagger e^{i\varphi_n\mathcal{N}}\mathcal{W}$. We stabilize the calculation by the method discussed in Appendix B.

A. The Hartree–Fock limit

In the limit in which the pairing condensate vanishes, i.e., $\Delta \to 0$, the HFB approximation reduces to the HF approximation. The matrix in Eq. (2) becomes diagonal, and the mean-field Hamiltonian can be rewritten as

$$\hat{H}_{\rm HF} = \sum_{ij} h_{ij} a_i^\dagger a_j. \tag{18}$$

In this limit, the Bogoliubov transformation reduces to a unitary transformation among the particle basis operators, and $\mathcal{V}$ vanishes. Because the particle-number operator is diagonal in a particle basis, $\mathcal{W}^\dagger e^{i\varphi_n\mathcal{N}}\mathcal{W} = e^{i\varphi_n\mathcal{N}}$. Equation (17) can then be written as

$$\begin{aligned}\zeta_n^{\rm HF} &= e^{\beta\langle\hat{V}\rangle}\det[1 + e^{-\beta h + (\beta\mu + i\varphi_n)}] \\ &= e^{\beta\langle\hat{V}\rangle}\prod_{k=1}^{N_s}[1 + e^{-\beta(\epsilon_k - \mu) + i\varphi_n}],\end{aligned} \tag{19}$$

where ϵ_k are the HF single-particle energies.

Equation (19) can be derived directly using $[\hat{H}_{\rm HF}, \hat{N}] = 0$ even when time-reversal symmetry is broken. A general derivation is given in Ref. [12].

B. The Bardeen–Cooper–Schrieffer limit

Equation (17) also simplifies in the BCS limit, in which the quasiparticle representation mixes particle state k with only its time-reversed counterpart $\bar{k}$. In this case, in the Bogoliubov transformation matrix given in Eq. (3), $\mathcal{U}$ is diagonal and $\mathcal{V}$ antidiagonal. Consequently, the transformation can be decomposed into a set of $N_s/2$ transformations

$$\begin{pmatrix}\alpha_k \\ \alpha_{\bar{k}}^\dagger\end{pmatrix} = \begin{pmatrix}u_k & -v_k \\ v_k & u_k\end{pmatrix}\begin{pmatrix}a_k \\ a_{\bar{k}}^\dagger\end{pmatrix} \tag{20}$$

for each pair $\{k, \bar{k}\}$ of time-reversed states. Here, u_k and v_k are real numbers satisfying $u_k^2 + v_k^2 = 1$. Equation (17) can then be rewritten as a product of 2×2 block determinants. Using

$$e^{i\varphi_n\mathcal{W}^\dagger\mathcal{N}\mathcal{W}}|_k = \begin{pmatrix}u_k^2 e^{i\varphi_n} + v_k^2 e^{-i\varphi_n} & u_k v_k(e^{i\varphi_n} - e^{-i\varphi_n}) \\ u_k v_k(e^{i\varphi_n} - e^{-i\varphi_n}) & v_k^2 e^{i\varphi_n} + u_k^2 e^{-i\varphi_n}\end{pmatrix} \tag{21}$$

for each block and $\prod_{k>0} e^{-i\varphi_n} = e^{i\varphi_n N_s/2} = (-)^n$, we find the final expression

$$\begin{aligned}\zeta_n^{\rm BCS} = e^{-\beta U_0}\prod_{k>0} e^{\beta E_k}\big[&u_k^2 + e^{2i\varphi_n}v_k^2 + 2e^{-\beta E_k + i\varphi_n} \\ &+ e^{-2\beta E_k}\big(v_k^2 + e^{2i\varphi_n}u_k^2\big)\big].\end{aligned} \tag{22}$$

The result in Eq. (22) can also be derived by writing explicitly the matrix elements of $e^{i\varphi_n\hat{N}}$ in the subspace spanned by the four many-body states $|\rangle_k = (u_k + v_k a_k^\dagger a_{\bar{k}}^\dagger)|\rangle$, $\alpha_k^\dagger|\rangle_k$, $\alpha_{\bar{k}}^\dagger|\rangle_k$, and $\alpha_k^\dagger\alpha_{\bar{k}}^\dagger|\rangle_k$, and evaluating the traces of $e^{i\varphi_n\hat{N}}e^{-\beta(\hat{H}_{\rm HFB} - \mu\hat{N} - \langle\hat{V}\rangle)}$ in each of these subspaces.

The result in Eq. (22) is given by Eqs. (24) and (25) of Ref. [15] but is obtained here as the special limit of a more general formula. A formula for the BCS limit as a product of the corresponding 2×2 determinants is also presented in Ref. [16].

An important case of the BCS limit is that of a spherical condensate, in which the angular-momentum quantum number j and the magnetic quantum number m are preserved by the Bogoliubov transformation. In this case, the quasiparticle energies for a given j are independent of m. If the single-particle model space does not include more than one shell with the same j, the Bogoliubov transformation is then of the form (20), where $|k\rangle = |jm\rangle$ and $|\bar{k}\rangle = \pm|j - m\rangle$, with $m = 1/2, -3/2, 5/2, -7/2, \ldots$ being the positive-signature states. The parameters $u_k = u_j$, $v_k = v_j$ are independent of m, and Eq. (22) simplifies to

$$\begin{aligned}\zeta_n^{\rm HFB} = e^{-\beta U_0}\prod_j e^{\beta(j+\frac{1}{2})E_j}\big[&u_j^2 + e^{2i\varphi_n}v_j^2 + 2e^{-\beta E_j + i\varphi_n} \\ &+ e^{-2\beta E_j}\big(v_j^2 + e^{2i\varphi_n}u_j^2\big)\big]^{j+\frac{1}{2}}.\end{aligned} \tag{23}$$

III. DISCRETE GAUSSIAN APPROXIMATIONS AND STATISTICAL QUANTITIES

A. Saddle-point and discrete Gaussian approximations

In this section, we describe briefly the discrete Gaussian (DG) approximations introduced in Ref. [7]. For more details, we refer the reader to Sec. II of Ref. [7]. The traditional method for calculating level densities from a grand-canonical finite-temperature mean-field theory is by a three-dimensional (3D) saddle-point approximation. Specifically, the state density is given by

$$\rho\big(E,N_p,N_n\big) \approx \frac{1}{(2\pi)^{3/2}} \left|\frac{\partial(E,N_p,N_n)}{\partial(\beta,\alpha_p,\alpha_n)}\right|^{-1/2} e^{S_{\rm gc}}, \tag{24}$$

where $S_{\rm gc}$ is the grand-canonical entropy calculated in the mean-field approximation and the energy and particle numbers are set equal to the derivatives of $\ln Z_{\rm gc}$ with respect to $-\beta$ and $\alpha_{p,n}$, respectively. Here $\alpha_{p,n} = \beta\mu_{p,n}$, where $\mu_{p,n}$ are the proton and neutron chemical potentials.

Two refinements to this standard procedure were introduced in Ref. [7]. The first refinement is to separate the $\alpha_{p,n}$ and β integrations in the 3D saddle-point approximation. The $\alpha_{p,n}$ integrations are carried out first, giving the approximate canonical partition function

$$\ln Z_c \approx \ln Z_{\rm gc} - \sum_{i=p,n} \alpha_i N_i - \ln\zeta, \tag{25}$$

where the correction factor ζ (obtained in the two-dimensional saddle-point approximation) is given by

$$\zeta = 2\pi \left|\frac{\partial(N_p,N_n)}{\partial(\alpha_p,\alpha_n)}\right|^{1/2}. \tag{26}$$

In a second step, the state density is obtained from the approximate canonical partition function in Eq. (25) by carrying out the β integration in the saddle-point approximation. The canonical entropy obtained in this procedure differs from $S_{\rm gc}$ not only through the inclusion of ζ but also through the dependence of ζ on β. It is given by

$$S_c \approx S_{\rm gc} - \ln\zeta - \beta\delta E, \tag{27}$$

where $\delta E = -d\ln\zeta/dE$. The approximate state density is given by an expression similar to the one given in Eq. (29) below. Equation (26) is derived by treating the particle numbers as continuous variables, and we therefore refer to this method as the continuous saddle-point approximation.

The next refinement to the standard 3D saddle-point approximation originates from the observation that N_p and N_n are discrete integers and should not be treated as continuous variables when the particle-number fluctuation is small. Specifically, the continuous saddle-point approximation breaks down when $2\pi\langle(\Delta N_i)^2\rangle \leqslant 1$ for $i = p, n$. This problem is dealt with in Ref. [7] by the introduction of the discrete Gaussian (DG) approximation, in which the correction factor ζ is not given by Eq. (26) but instead by

$$\zeta = \sum_{N_i',N_j'} \exp\left(-\frac{1}{2}\sum_{i,j}\left.\frac{\partial N}{\partial\alpha}\right|^{-1}_{ij}(N_i'-N_i)(N_j'-N_j)\right), \tag{28}$$

where $i, j = p, n$. In the DG approximation, ζ is guaranteed to be at least unity, so this approximation will not break down when the particle-number fluctuation is small. When the particle-number fluctuation is large, the DG correction factor in Eq. (28) agrees with the continuous saddle-point correction factor in Eq. (26).

In Ref. [7], two versions of the DG approximation were introduced. In the first, which we call DG1, the matrix $\partial N/\partial\alpha$ is determined numerically. In the second, which we call DG2, the matrix $\partial N/\partial\alpha$ is replaced by a diagonal matrix whose diagonal elements are given by the particle-number variances $\langle(\Delta N_i)^2\rangle$ calculated in the grand-canonical mean-field theory. Because it neglects the potentially nonzero off-diagonal terms, DG2 is expected to be less accurate than DG1 at low temperatures.

B. Canonical energy, entropy, and state density

We summarize here the formulas used to find the statistical quantities calculated in Sec. IV. Given the canonical partition function Z_c, the average state density $\rho(E)$ at energy E is evaluated by a one-dimensional (1D) saddle-point approximation as

$$\rho(E) \approx \left(2\pi\left|\frac{\partial E}{\partial\beta}\right|\right)^{-1/2} e^{S_c(\beta)}, \tag{29}$$

where β is determined as a function of the energy E by the saddle-point condition $E = -\partial\ln Z_c/\partial\beta = E_c$ and S_c is the canonical entropy $S_c = \ln Z_c + \beta E_c$. When $Z_c(\beta)$ is the exact canonical partition function $Z_c(\beta) = {\rm Tr}\,(\hat{P}_N e^{-\beta\hat{H}})$ (here $\hat{P}_N = \hat{P}_{N_p}\hat{P}_{N_n}$, with N_p and N_n being the numbers of protons and neutrons, respectively), $E_c = {\rm Tr}\,(\hat{P}_N e^{-\beta\hat{H}}\hat{H})/Z_c(\beta)$ and $S_c = -{\rm Tr}\,(\hat{D}_N\ln\hat{D}_N)$ are, respectively, the exact canonical energy and entropy of the correlated density matrix $\hat{D}_N = \hat{P}_N e^{-\beta\hat{H}}/Z_c(\beta)$.

In the particle-number-projected HFB approximation, $Z_c^{\rm HFB} = Z_{N_p}^{\rm HFB} Z_{N_n}^{\rm HFB}$, where $Z_{N_{p(n)}}^{\rm HFB}$ is given by Eqs. (9) and (17). The approximate canonical HFB energy $E_c^{\rm HFB}$ is determined by the saddle-point condition

$$E = -\frac{\partial\ln Z_c^{\rm HFB}}{\partial\beta} = E_c^{\rm HFB}, \tag{30}$$

and the approximate canonical HFB entropy is

$$S_c^{\rm HFB} = \ln Z_c^{\rm HFB} + \beta E_c^{\rm HFB}. \tag{31}$$

The average state density in the HFB approximation is then given by Eq. (29) with the canonical energy and entropy replaced by the their HFB expressions (30) and (31).

We note that the above $E_c^{\rm HFB}$ differs from the expectation value of $\hat{H}$ in the particle-number projected HFB density operator $\hat{D}_N^{\rm HFB} = \hat{P}_N e^{-\beta(\hat{H}_{\rm HFB}-\langle\hat{V}\rangle)}/Z_N^{\rm HFB}$, and similarly $S_c^{\rm HFB} \neq -{\rm Tr}\,(\hat{D}_N^{\rm HFB}\ln\hat{D}_N^{\rm HFB})$. The reason for these differences is the explicit dependence of $\hat{H}_{\rm HFB}$ on the grand-canonical one-body density and pairing tensor.

In the DG approximations, $\ln Z_c$ is given by Eq. (25), where ζ is given by Eq. (28). The energy is given by the saddle-point condition (30), and the entropy by Eq. (31), where $Z_c^{\rm HFB}$ is replaced by the DG1 or DG2 partition function.

IV. RESULTS

Here we present results for the particle-number-projected finite-temperature mean-field theories in three heavy nuclei. In this section, we refer to the particle-number projection as the PNP method. First, we discuss ^{162}Dy, a typical strongly deformed nucleus for which the appropriate mean-field theory is the HF approximation. Next, we present results for ^{148}Sm, a typical spherical nucleus with a strong pairing condensate for which the BCS limit of the HFB is appropriate. Finally, we discuss a transitional nucleus ^{150}Sm, in which the pairing condensate is deformed and the general projection formula (17) is required. The results from the PNP are compared with the discrete Gaussian approximations of Ref. [7] and with the SMMC results [17,18].

The Hamiltonian for these calculations is taken from Refs. [17,18], where the original calculations of the SMMC level density were carried out. It is given in a shell-model basis having $N_s = 40$ proton orbitals and $N_s = 66$ neutron orbitals.

A. Particle-number-projected Hartree–Fock for strongly deformed nucleus: ^{162}Dy

We applied the particle-number-projected HF approximation to the strongly deformed nucleus ^{162}Dy, in which the pairing is weak, by using Eqs. (9) and (19) to calculate the particle-number-projected partition function. In Fig. 1, we compare the approximate canonical entropy (31) from the PNP with those from the DG approximations and with the SMMC entropy. The kink at $\beta \approx 0.83$ MeV^{-1} in the HF results is due to the sharp shape transition that occurs in the grand-canonical HF approximation. At β values below the shape transition (i.e., in the spherical phase), the HF results are in good agreement with those from the SMMC. However, at β values above the shape transition, the entropies from the PNP and the DG approximations are noticeably lower than the SMMC entropy. The reason for this discrepancy is that the HF approximation accounts only for the intrinsic K states and not for the rotational bands that are built on top of these intrinsic states.

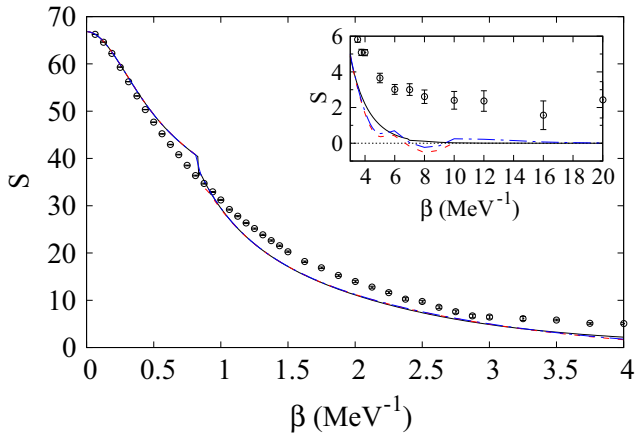

FIG. 1. Canonical entropy of ^{162}Dy vs β in the HF approximation. The approximate PNP canonical entropy (31) (solid black line) is compared with the approximate canonical entropy from DG1 (dashed red line) and from DG2 (dashed-dotted blue line). The open circles represent the SMMC entropy. The inset shows the various entropies at higher β values.

The PNP, DG1, and DG2 give nearly identical results for $\beta < 4$ MeV^{-1}. In DG1 and DG2, however, the entropy exhibits unphysical oscillatory behavior for $4 \leqslant \beta \leqslant 10$ MeV^{-1}. In contrast, the entropy asymptotes monotonically to zero at large β in the PNP, as would be physically expected.

The PNP canonical excitation energy and state density closely resemble the corresponding results for the DG approximations, which are shown in Figs. 6 and 10 of Ref. [7]. The deviation between the PNP entropy and the DG entropy observed at low temperatures does not lead to any significant difference in the state densities. Figures showing these observables are included in the Supplemental Material [14].

B. Particle-number-projected Hartree–Fock–Bogoliubov for spherical condensate: ^{148}Sm

To test our formulas for the particle-number-projected HFB partition function in the BCS limit, given by Eqs. (9) and (23), we apply the particle-number-projected HFB approximation to ^{148}Sm, for which the pairing condensate is spherical. The canonical entropies for the PNP, the DG approximations, and the SMMC are shown in Fig. 2. The kinks in the HFB results in the region $2 \leqslant \beta \leqslant 3$ MeV^{-1} are due to the proton and neutron pairing transitions. For β values below the first pairing transition, there is good agreement between the HFB results and the SMMC results. The kinks that indicate the pairing transitions are more pronounced in the PNP and DG2 than in DG1.

In the paired phase, the approximate canonical entropies for the PNP and the DG approximations decrease rapidly, dropping below zero around $\beta \approx 4$ MeV^{-1}. A negative entropy is unphysical because the entropy of a nondegenerate ground state is zero. This negative entropy originates in the intrinsic violation of particle-number conservation in the grand-canonical HFB approximation and will be explained for the PNP in

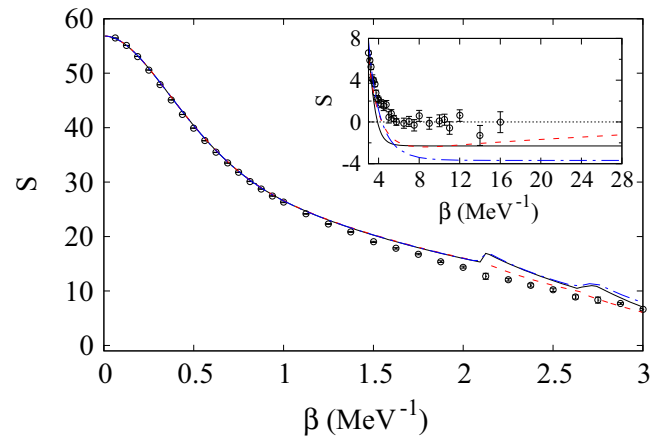

FIG. 2. Canonical entropies of ^{148}Sm vs β in the BCS limit of the HFB approximation. Lines and symbols are as in Fig. 1. The inset shows the entropies for higher β values.

Sec. IV D. An explanation for the DG approximations was given in Ref. [7].

However, for large β values, the PNP exhibits qualitative and quantitative improvements over the DG approximations. The entropy from the PNP asymptotes smoothly to a value of $S_c \approx -2.30$. The entropy from DG1 reaches a minimum around $\beta \approx 8\,\mathrm{MeV}^{-1}$ and subsequently increases with increasing β. Such an increase is unphysical because, for these values of β, the system is already in its ground state. The entropy from DG2 asymptotes smoothly to a negative value of $S_c \approx -3.68$. The absolute error in the estimate for the ground-state entropy is thus larger in DG2 than in the PNP by more than a unit.

At small and intermediate values of β, the PNP excitation energy for ^{148}Sm closely resembles the DG1 excitation energy shown in Fig. 13 of Ref. [7]. The PNP state density is similar to the DG2 state density shown by the dotted line in Fig. 16 of Ref. [7] while the DG1 state density is somewhat enhanced at low excitation energies. Figures showing these observables are included in the Supplemental Material [14].

C. Particle-number-projected Hartree–Fock–Bogoliubov for deformed condensate: ^{150}Sm

To calculate the particle-number-projected HFB partition function for ^{150}Sm, which has a deformed pairing condensate, we must use the general PNP HFB formalism of Sec. II, i.e., Eqs. (9) and (17). In this case, the advantages of the PNP over the DG approximations are significant for the excitation energy, canonical entropy, and state density. In particular, DG1, the more accurate of the two DG methods used in Ref. [7], becomes numerically unstable for temperatures below the shape transition. Because of this instability, we omit DG1 from the figures in this section. In contrast, the PNP remains stable for all temperatures.

1. Excitation energy

In Fig. 3, we show the excitation energy as a function of β for the PNP and DG2 in comparison with the SMMC energy. The kink at $\beta \approx 1.5\ \mathrm{MeV}^{-1}$ is the shape transition, and the kinks at $\beta \approx 3\ \mathrm{MeV}^{-1}$ and $\beta \approx 6\ \mathrm{MeV}^{-1}$ are the proton and neutron pairing transitions, respectively. Except around the phase transitions, there is good agreement between the PNP and DG2 results and the SMMC results. The DG2 approximation shows a larger discrepancy from the SMMC around the pairing transitions than does the PNP.

2. Canonical entropy

The canonical entropies from the PNP, DG2 and SMMC are shown in Fig. 4. At β values below the shape transition, there is close agreement between the SMMC and the HFB results. Between the shape transition at $\beta \approx 1.5\ \mathrm{MeV}^{-1}$ and the proton pairing transition at $\beta \approx 3\,\mathrm{MeV}^{-1}$, the PNP and DG2 entropies are lower than the SMMC entropy because of the contributions of rotational bands to the SMMC. For β values above the proton pairing transition, the HFB entropies are reduced even further, falling below zero above $\beta \approx 4\,\mathrm{MeV}^{-1}$. As in the case of ^{148}Sm, this negative entropy originates in the violation of particle-number conservation in the HFB approximation.

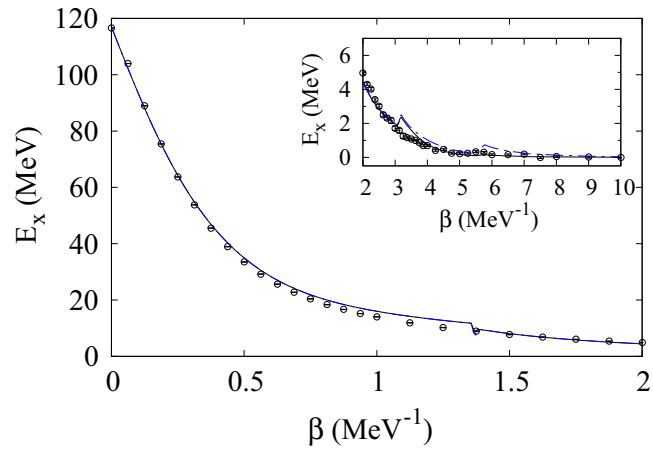

FIG. 3. Excitation energy of ^{150}Sm vs β in the HFB approximation. The approximate canonical energy calculated from the PNP (solid black line) is compared with the approximate canonical energy from DG2 (dashed-dotted blue line). DG1 becomes unstable for this nucleus and is not shown. The open circles are the SMMC excitation energies. The inset shows higher β values.

The entropy from the PNP is very close to that from DG2 in the unpaired phase but shows a quantitative improvement over DG2 in the paired phase. The entropy from the PNP asymptotes to $S_c \approx -1.20$, while the entropy from DG2 asymptotes to $S_c \approx -2.52$. As with ^{148}Sm, the absolute error of the ground-state entropy in the PNP is lower by more than a unit of entropy than the error in DG2. Furthermore, DG2 shows a large spike near the neutron pairing transition, which is not present in the PNP.

3. State density

The behavior of the state density, which is shown for the PNP, DG2 and SMMC in Fig. 5, closely resembles that of the canonical entropy. At energies above the shape transition, the PNP and DG2 results agree well with the SMMC results. The

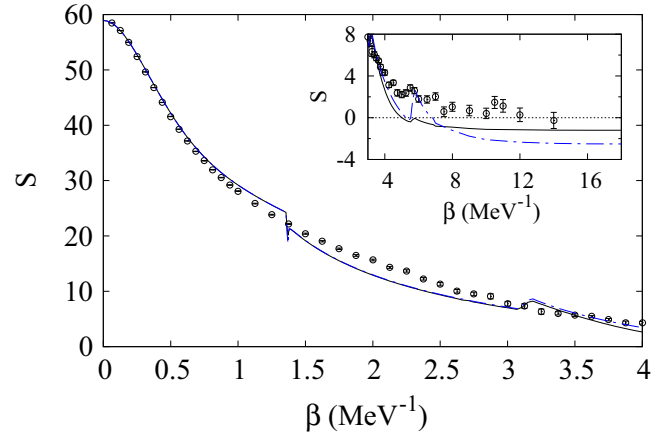

FIG. 4. Canonical entropy of ^{150}Sm vs β in the HFB approximation. Lines and symbols for the PNP, DG2, and SMMC are as in Fig. 3. The inset shows an expanded scale at large values of β.

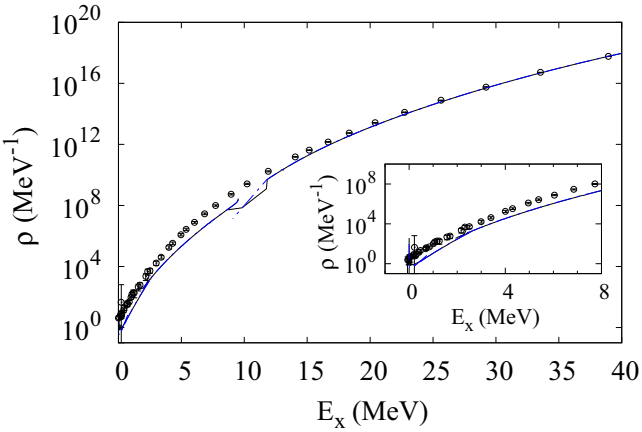

FIG. 5. State density of ^{150}Sm vs excitation energy E_x in the HFB approximation. Lines and symbols are as in Fig. 3. The inset shows the low-excitation-energy results.

HFB results are reduced at energies below the shape transition and reduced further at energies below the pairing transitions. The discontinuities in both the PNP and in DG2 around $E_x \approx 10$ MeV are due to the sharp kink in the excitation energy at the shape transition. The discrepancy between the PNP and DG2 entropies in the high-β limit is not noticeable in the state density because this discrepancy becomes significant only for very low excitation energies.

D. Approximate canonical Hartree–Fock–Bogoliubov entropy in limit $T \to 0$

We found in Secs. IV B and IV C that the approximate canonical entropy of ^{148}Sm and ^{150}Sm asymptotes at low temperatures to a negative number. Here, we show how this unphysical result arises from the inherent violation of particle-number conservation in the grand-canonical HFB approximation. We consider the limit of sufficiently large β, in which we can neglect the contribution of excited states to the partition function. Assuming for simplicity one type of particle, we have in this limit

$$Z_N^{\mathrm{HFB}} \to e^{-\beta E_0} \langle \Phi | \hat{P}_N | \Phi \rangle, \tag{32}$$

where E_0 is the ground-state energy and $|\Phi\rangle$ is the HFB ground state. This state can be written as a linear superposition of states with even particle numbers, $|\Phi\rangle = \sum_{N=0,2,4,\ldots} \alpha_N |\psi\rangle_N$, where $|\psi\rangle_N$ is an N-particle state. Equation (32) can then be expressed as

$$Z_N^{\mathrm{HFB}} \to e^{-\beta E_0} |\alpha_N|^2. \tag{33}$$

where $|\alpha_N|^2$ is the probability that the HFB ground-state condensate contains N particles. Using Eq. (31) and generalizing to the case of both protons and neutrons, we find in the limit of zero temperature

$$S_c^{\mathrm{HFB}} \to \ln |\alpha_{N_p}|^2 + \ln |\alpha_{N_n}|^2, \tag{34}$$

where N_p and N_n are the numbers of protons and neutrons, respectively. Because particle-number is not conserved, $|\alpha_{N_p}|^2, |\alpha_{N_n}|^2 < 1$, and the entropy (34) is negative. A closely related explanation for the DG approximations is given in Ref. [7]. This negative entropy is an inherent limitation of the particle-number projection after variation method in the grand-canonical HFB theory.

E. Computational efficiency

An important advantage of the PNP over all saddle-point methods in which the partial derivatives are calculated explicitly is computational efficiency. Both the PNP and these saddle-point methods require finding the self-consistent mean-field solutions for a set of β values. The additional cost of the PNP HF approximation scales as N_s^2, since calculating ζ_n^{HF} in Eq. (19) takes N_s operations and must be done for each of the N_s quadrature points in the Fourier sum. The PNP HFB approximation scales as N_s^4 because the matrix decomposition in the stabilization method (discussed in Appendix B) requires N_s^3 operations for each of the N_s quadrature points.

In DG1 it is necessary to calculate numerically the derivatives of the proton and neutron numbers with respect to the chemical potentials, which requires finding additional mean-field solutions. The cost of calculating these derivatives accurately can be very large, especially in the vicinity of the phase transitions where the mean-field solution can take many iterations to converge. These timing considerations do not apply to DG2, since in that approximation the relevant derivatives are replaced by the particle-number variances calculated as mean-field observables. However, as discussed in Ref. [7], DG2 is significantly less accurate than DG1 in the paired phase. In contrast, the PNP is as accurate or more accurate than DG1 in each of the nuclei considered here.

In the Supplemental Material [14], we include timing data comparing the efficiency of the PNP to that of the DG1 approximation for the spherical nucleus ^{148}Sm.

V. CONCLUSION AND OUTLOOK

We have derived a general formula for exact particle-number projection after variation in the finite-temperature HFB approximation, assuming only that the HFB Hamiltonian is invariant under time reversal. This general formula reduces to simpler known expressions in the HF and BCS limits.

We have assessed the accuracy of the PNP, using the SMMC as a benchmark. In addition, we have compared the performance of this method to the DG approximations formulated in Ref. [7], which were introduced to improve on the saddle-point approximation. Our results show that, like the DG approximations, the PNP is in agreement with the SMMC for temperatures above the shape or pairing phase transitions. In general, we find that the PNP provides both quantitative and qualitative improvements over the DG and saddle-point approximations at low temperatures. In the HF case, the PNP suppresses an instability that develops in the canonical entropy calculated by the DG approximations at large β. In the paired phase of the HFB, the PNP entropy shows the correct qualitative behavior, i.e., it is monotonically decreasing with increasing β, unlike the DG1 approximation. Furthermore, in the paired phase, the PNP reduces the error

in the DG2 approximation by more than a unit of entropy. This reduction is significant, since the errors in both cases are of order unity. Finally, the PNP is significantly more computationally efficient than saddle-point methods in which derivatives have to be calculated explicitly, such as the DG1 approximation.

However, the PAV method is inherently limited by the broken symmetries in the grand-canonical mean-field theory to which it is applied. In a deformed nucleus, the projected mean-field theory cannot describe the rotational enhancement that is observed in the SMMC below the shape transition temperature. In a nucleus with a strong pairing condensate, the intrinsic violation of particle-number conservation below the pairing transition temperature leads to negative values of the PNP canonical entropy. It is therefore desirable to explore improvements to finite-temperature mean-field theories that can address these issues.

One avenue for improvement is the variation after projection (VAP) method. VAP conserves particle number during the variation to determine the mean-field solution and is therefore expected to smooth the sharp phase transitions of the grand-canonical mean-field approximations and correct the unphysical negative entropy in the paired phase. This method has been formulated for the zero-temperature HFB approximation [19] and applied to even-even nuclei [20,21]. VAP has also been formulated at finite temperature in the BCS approximation to calculate the pairing gaps in small model spaces [22,23]. However, a general VAP method for finite-temperature calculations in large model spaces would involve a considerable computational cost. In particular, the entropy of the projected HFB density $S_N = -\mathrm{Tr}\,(\hat{D}_N \ln \hat{D}_N)$, which is required for the calculation of the free energy at finite temperature, is difficult to calculate in the paired phase because the HFB Hamiltonian does not commute with the particle-number operator. Nevertheless, given the potential advantages of this method, it would be worth investigating the possibility of developing a general VAP method for the finite-temperature HF and HFB approximations in large model spaces.

Another direction, perhaps more tractable, would be to use the PNP in the static-path approximation (SPA) [24–27]. The SPA takes into account the static fluctuations of the mean field beyond its self-consistent solution. As with the mean-field approximation, the particle-number projection can be carried out either before or after the SPA integration. It would be useful to conduct a systematic assessment of the particle-number-projected SPA.

Finally, the formula derived here for the particle-number projected HFB partition function assumes that the HFB Hamiltonian is time-reversal invariant and therefore is not completely general. A general formula for the projected HFB partition function was derived in Ref. [12], but its application is limited by a sign ambiguity. For the grand-canonical traces of statistical density operators, a similar sign ambiguity was resolved by relating the trace over Fock space to a Pfaffian [28]. An extension of the Pfaffian approach to symmetry restoration projection at finite temperature for a general HFB Hamiltonian, and specifically for particle-number projection, will be presented in Ref. [29].

ACKNOWLEDGMENTS

This work was supported in part by the U.S. DOE Grants No. DE-FG02-91ER40608 and No. DE-FG02-00ER411132.

APPENDIX A: TRACE OF EXPONENTIAL OF FERMIONIC ONE-BODY OPERATOR

Here, we derive the formula for the grand-canonical trace of the exponential of a quadratic fermionic operator of the form of Eq. (6). Assuming a diagonalizable $N_s \times N_s$ matrix $\mathcal{C}$,

$$\mathrm{Tr}\, e^{\xi^\dagger \mathcal{C} \xi} = \det(1 + e^{\mathcal{C}}), \tag{A1}$$

where ξ is defined in Sec. II.

Since $\mathcal{C}$ is diagonalizable, there is a similarity transformation S that brings $\mathcal{C}$ to a diagonal form,

$$S\mathcal{C}S^{-1} = \begin{pmatrix} \lambda_{k_1} & & & & & & \\ & \ddots & & & & & \\ & & \lambda_{k_{N_s/2}} & & & & \\ & & & \lambda_{\bar{k}_1} & & & \\ & & & & \ddots & & \\ & & & & & \lambda_{\bar{k}_{N_s/2}} & \end{pmatrix}. \tag{A2}$$

If S is unitary, it can be used to transform α_k and $\alpha_k^\dagger$ to new fermionic operators d_k and $d_k^\dagger$ such that

$$\begin{aligned} \mathrm{Tr}\, e^{\xi^\dagger \mathcal{C} \xi} &= \mathrm{Tr}\, e^{\sum_{k>0}(\lambda_k d_k^\dagger d_k + \lambda_{\bar{k}} d_{\bar{k}} d_{\bar{k}}^\dagger)} \\ &= \mathrm{Tr}\, e^{\sum_{k>0}(\lambda_k d_k^\dagger d_k - \lambda_{\bar{k}} d_{\bar{k}}^\dagger d_{\bar{k}} + \lambda_{\bar{k}})}. \end{aligned} \tag{A3}$$

Since d_k are fermionic operators, the grand-canonical trace in Eq. (A3) can be evaluated as usual to give

$$\begin{aligned} \mathrm{Tr}\, e^{\xi^\dagger \mathcal{C} \xi} &= \prod_{k>0} [(1 + e^{\lambda_k})(1 + e^{-\lambda_{\bar{k}}}) e^{\lambda_{\bar{k}}}] \\ &= \prod_{k>0} [(1 + e^{\lambda_k})(1 + e^{\lambda_{\bar{k}}})] = \det(1 + e^{\mathcal{C}}). \end{aligned} \tag{A4}$$

However, in general, S is not unitary. In this case, we make use of a nonunitary Bogoliubov transformation [30]. We define the operators $\{d, \tilde{d}\}$ by the canonical transformation

$$\eta = S\xi, \quad \tilde{\eta} = \xi^\dagger S^{-1}, \tag{A5}$$

where $\eta = (d_{k_1}, \ldots, d_{k_{N_s/2}}, \tilde{d}_{\bar{k}_1}, \ldots, \tilde{d}_{\bar{k}_{N_s/2}})^T$ and $\tilde{\eta} = (\tilde{d}_{k_1}, \ldots, \tilde{d}_{k_{N_s/2}}, d_{\bar{k}_1}, \ldots, d_{\bar{k}_{N_s/2}})$. It can be shown that $\{d, \tilde{d}\}$ have the same anticommutation relations as $\{\alpha, \alpha^\dagger\}$ [30]. However, this transformation does not preserve the Hermiticity relation of the operators. Therefore we must treat the kets and bras related to these operators differently. Because the anticommutation relations are preserved, the usual creation and annihilation formulas apply to the left and right bases

separately. We define the left and right vacuums by

$$|0\rangle_d = \prod_{k>0} d_k d_{\bar{k}}|0\rangle, \quad {}_d\langle\bar{0}| = \langle 0|\prod_{k>0}\tilde{d}_k\tilde{d}_{\bar{k}}, \tag{A6}$$

and left and right states by

$$|\phi\rangle = \prod_{k>0}(\tilde{d}_k)^{n_k}(\tilde{d}_{\bar{k}})^{n_{\bar{k}}}|0\rangle_d,$$
$$\langle\bar{\phi}| = {}_d\langle\bar{0}|\prod_{k>0}(d_k)^{n_k}(d_{\bar{k}})^{n_{\bar{k}}}. \tag{A7}$$

The anticommutation relations ensure that

$$\langle\bar{\phi}|\phi'\rangle = \delta_{\phi,\phi'}, \quad \langle\bar{\phi}|\tilde{d}_k d_k|\phi\rangle = n_k, \tag{A8}$$

where n_k is the occupation number of state k. Furthermore, as discussed in Ref. [30], these left and right states form a bi-orthogonal basis for the Fock space and therefore satisfy the completeness relation,

$$\sum_{\phi}|\phi\rangle\langle\bar{\phi}| = 1. \tag{A9}$$

We can rewrite $\xi^\dagger\mathcal{C}\xi$ in this bi-orthogonal basis,

$$\xi^\dagger\mathcal{C}\xi = \tilde{\eta}S\mathcal{C}S^{-1}\eta = \sum_{k>0}\lambda_k\tilde{d}_k d_k - \lambda_{\bar{k}}\tilde{d}_{\bar{k}}d_{\bar{k}} + \lambda_{\bar{k}}. \tag{A10}$$

We can now compute the trace as follows ($|\psi\rangle$ below is an arbitrary state in the $\alpha, \alpha^\dagger$ basis):

$$\begin{aligned}\mathrm{Tr}\, e^{\xi^\dagger\mathcal{C}\xi} &= \sum_{\psi}\langle\psi|e^{\xi^\dagger\mathcal{C}\xi}|\psi\rangle \\ &= \sum_{\psi,\phi,\phi'}\langle\psi|\phi\rangle\langle\bar{\phi}|e^{\sum_{k>0}(\lambda_k\tilde{d}_k d_k - \lambda_{\bar{k}}\tilde{d}_{\bar{k}}d_{\bar{k}}+\lambda_{\bar{k}})}|\phi'\rangle\langle\bar{\phi}'|\psi\rangle \\ &= \sum_{\phi}\langle\bar{\phi}|\prod_{k>0}e^{(\lambda_k\tilde{d}_k d_k - \lambda_{\bar{k}}\tilde{d}_{\bar{k}}d_{\bar{k}}+\lambda_{\bar{k}})}|\phi\rangle \\ &= \prod_{k>0}\sum_{\substack{n_k=0,1\\ n_{\bar{k}}=0,1}} e^{\lambda_k n_k + \lambda_{\bar{k}}(1-n_{\bar{k}})} \\ &= \prod_{k>0}(1+e^{\lambda_k})(1+e^{\lambda_{\bar{k}}}) = \det(1+e^{\mathcal{C}}).\end{aligned} \tag{A11}$$

This completes the proof of Eq. (A1).

APPENDIX B: STABILIZATION OF HARTREE–FOCK–BOGOLIUBOV PARTICLE-NUMBER PROJECTION

Equation (17) becomes numerically unstable at large values of β. We rewrite

$$\begin{aligned}&\det(1+\mathcal{W}^\dagger e^{i\varphi_n\mathcal{N}}\mathcal{W}e^{-\beta\mathcal{E}}) \\ &\quad = \det(\mathcal{W}^\dagger)\det(e^{i\varphi_n\mathcal{N}})\det(\mathcal{W})\det(\mathcal{W}^\dagger e^{-i\varphi_n\mathcal{N}}\mathcal{W}+e^{-\beta\mathcal{E}}).\end{aligned} \tag{B1}$$

Using $\det(e^{i\varphi_n\mathcal{N}}) = 1$ and $\det\mathcal{W}^\dagger = [\det\mathcal{W}]^{-1}$, we find

$$\det(1+\mathcal{W}^\dagger e^{i\varphi_n\mathcal{N}}\mathcal{W}e^{-\beta\mathcal{E}}) = \det(\mathcal{W}^\dagger e^{-i\varphi_n\mathcal{N}}\mathcal{W}+e^{-\beta\mathcal{E}}). \tag{B2}$$

The determinant on the right-hand side can be computed stably [31] by decomposing the matrix $A_n \equiv \mathcal{W}^\dagger e^{-i\varphi_n\mathcal{N}}\mathcal{W} + e^{-\beta\mathcal{E}}$ in the form

$$A_n = Q_n D_n R_n, \tag{B3}$$

where Q_n is an orthogonal matrix, R_n is an upper triangular matrix in which each diagonal entry is 1, and D_n is a diagonal matrix. Q_n and R_n are well-conditioned matrices, while D_n contains the scales of the problem. Consequently, the eigenvalues of Q_n and R_n can be computed stably. We use these eigenvalues, together with the diagonal entries of D_n, to find $\det A_n$. In practice, to avoid numerical overflow, we compute the quantity

$$\ln\det A_n = \ln\det Q_n + \ln\det D_n + \ln\det R_n. \tag{B4}$$

[1] A. L. Goodman, Nucl. Phys. A **352**, 30 (1981).
[2] K. Tanabe, K. Sugawara-Tanabe, and H. J. Mang, Nucl. Phys. A **357**, 20 (1981).
[3] S. Hilaire and S. Goriely, Nucl. Phys. A **779**, 63 (2006).
[4] T. Ericson, Adv. Phys. **9**, 425 (1960).
[5] A. Bohr and B. Mottelson, *Nuclear Structure* (Benjamin, New York, 1975), Vol. I.
[6] A. K. Kerman and S. Levit, Phys. Rev. C **24**, 1029 (1981).
[7] Y. Alhassid, G. F. Bertsch, C. N. Gilbreth, and H. Nakada, Phys. Rev. C **93**, 044320 (2016).
[8] G. H. Lang, C. W. Johnson, S. E. Koonin, and W. E. Ormand, Phys. Rev. C **48**, 1518 (1993).
[9] Y. Alhassid, D. J. Dean, S. E. Koonin, G. H. Lang, and W. E. Ormand, Phys. Rev. Lett. **72**, 613 (1994).
[10] For a recent review, see Y. Alhassid, arXiv:1607.01870; *Emergent Phenomena in Atomic Nuclei from Large-Scale Modeling: A Symmetry-Guided Perspective*, edited by K. D. Launey (World Scientific, Singapore, 2017).
[11] P. Ring and P. Schuck, *The Nuclear Many-Body Problem* (Springer-Verlag, New York, 1980).
[12] R. Rossignoli and P. Ring, Ann. Phys. (NY) **235**, 350 (1994).
[13] K. Tanabe and H. Nakada, Phys. Rev. C **71**, 024314 (2005).
[14] See Supplemental Material at http://link.aps.org/supplemental/10.1103/PhysRevC.96.014305 for the particle-number projection codes, the data files used to produce all figures shown, and additional figures.
[15] C. Esebbag and J. L. Egido, Nucl. Phys. A **552**, 205 (1993).
[16] H. Flocard, in *Atomic Clusters and Nanoparticles* (Les Houches, Session LXXIII), edited by C. Guet, P. Hobza, F. Spiegelman, and F. David (Springer, Heidelberg, 2001).
[17] Y. Alhassid, L. Fang, and H. Nakada, Phys. Rev. Lett. **101**, 082501 (2008).
[18] C. Özen, Y. Alhassid, and H. Nakada, Phys. Rev. Lett. **110**, 042502 (2013).
[19] J. Sheikh and P. Ring, Nucl. Phys. A **665**, 71 (2000).
[20] M. Anguiano, J. Egido, and L. M. Robledo, Nucl. Phys. A **696**, 467 (2001).
[21] M. V. Stoitsov, J. Dobaczewski, R. Kirchner, W. Nazarewicz, and J. Terasaki, Phys. Rev. C **76**, 014308 (2007).
[22] D. Gambacurta and D. Lacroix, Phys. Rev. C **85**, 044321 (2012).

[23] D. Gambacurta, D. Lacroix, and N. Sandulescu, Phys. Rev. C **88**, 034324 (2013).
[24] B. Mühlschlegel, D. J. Scalapino, and R. Denton, Phys. Rev. B **6**, 1767 (1972).
[25] Y. Alhassid and J. Zingman, Phys. Rev. C **30**, 684 (1984).
[26] B. Lauritzen, P. Arve, and G. F. Bertsch, Phys. Rev. Lett. **61**, 2835 (1988).
[27] G. Puddu, P. F. Bortignon, and R. A. Broglia, Ann. Phys. (NY) **206**, 409 (1991).
[28] L. M. Robledo, Phys. Rev. C **79**, 021302(R) (2009).
[29] P. Fanto (unpublished).
[30] R. Balian and E. Brezin, Nuovo Cimento B **64**, 37 (1969).
[31] E. Y. Loh, Jr. and J. E. Gubernatis, in *Electronic Phase Transitions*, edited by W. Hanke and Y. V. Kopaev (North Holland, Amsterdam, 1992).